Comments on Inorganic Chemistry
Publication details, including instructions for authors and subscription information:
http://www.informaworld.com/smpp/title~content=t713455155

MOLECULAR DESIGN, SYNTHESIS AND STRUCTURE-PROPERTY RELATIONSHIP OF OLIGOTHIOPHENE-DERIVED METALLAYNES

Wai-Yeung Wong[a]
[a] Department of Chemistry and Centre for Advanced Luminescence Materials, Hong Kong Baptist University, Hong Kong, P.R. China

To cite this Article Wong, Wai-Yeung(2005) 'MOLECULAR DESIGN, SYNTHESIS AND STRUCTURE-PROPERTY RELATIONSHIP OF OLIGOTHIOPHENE-DERIVED METALLAYNES', Comments on Inorganic Chemistry, 26: 1, 39 — 74
To link to this Article: DOI: 10.1080/02603590590920514
URL: http://dx.doi.org/10.1080/02603590590920514

Comments on Inorganic Chemistry, 26: 39–74, 2005

ISSN: 0260-3594 print
DOI: 10.1080/02603590590920514

Taylor & Francis
Taylor & Francis Group

MOLECULAR DESIGN, SYNTHESIS AND STRUCTURE-PROPERTY RELATIONSHIP OF OLIGOTHIOPHENE-DERIVED METALLAYNES

WAI-YEUNG WONG

Department of Chemistry and Centre for Advanced Luminescence Materials, Hong Kong Baptist University, Hong Kong, P.R. China

A series of conjugated bimetallic complexes and their polymeric analogues containing alkyne-functionalized α-coupled oligothiophenes have been synthesized and characterized. The introduction of transition metal centers, with their large variety of ligand environments and oxidation states, can impart interesting physical, optoelectronic and structural properties on these oligothiophene systems. It was demonstrated that π-conjugation of organometallic alkynyl units into the oligothiophene chain offers intriguing models that possess unique features that are not accessible in the classical organic counterparts. The photophysical, electrochemical and structural properties of these classes of metallaynes have been extensively investigated in terms of the type of metal centers and the number of oligothienyl rings within the bridging ligand. The experimental results have also been correlated to the theoretical data obtained by molecular orbital calculations using density functional theory.

***Keywords*: metallaynes, oligothiophenes, cobalt(0), platinum(II), ferrocenyl, gold(I), mercury(II), bithiazoles**

Address correspondence to Wai-Yeung Wong, Department of Chemistry and Centre for Advanced Luminescence Materials, Hong Kong Baptist University, Waterloo Road, Kowloon Tong, Hong Kong, P.R. China. E-mail: rwywong@hkbu.edu.hk

1. INTRODUCTION

The preparation and physical studies of metal-based conjugated organic materials and polymers have been the subject of significant research interest in the past few decades because of their possible applications in the materials industry.[1] The driving force for this work lies in the possibility of coupling the chemical, optical and electronic properties of metal complexes to those of the organic backbone, thus accessing novel materials with new properties. Among the vast majority of organic backbones used, conjugated thiophene derivatives have been extensively explored due to their chemical stability and synthetic accessibility (Figure 1).[2] It has been well documented that α-coupled oligothiophenes are attracting considerable attention in the rapidly expanding field of electronic and optoelectronic devices such as field-effect transistors (FETs)[3] and light-emitting diodes (LEDs),[4] and as the fluorescent biomarkers in biological research.[5] Polythiophene and its derivatives work very well in some of the above applications and remain one of the most versatile conjugated polymer systems. Moreover, highly organized molecular assemblies based on the thiophene oligomers have also been widely studied.[6] Although the $-C{\equiv}CC_6H_4C{\equiv}C-$ unit has been extensively used as the π-spacer in organic and homo- and heterometallic oligomers and polymers,[7] increasing attention is currently being paid to materials based on oligothiophenes and polythiophenes because of their remarkable electronic and optoelectronic properties.[3,4,8] The ease of modification and knowledge in the structure-property relationship of polythiophenes continues to make the synthesis of oligo- and polythiophenes a critical subject in the development of new

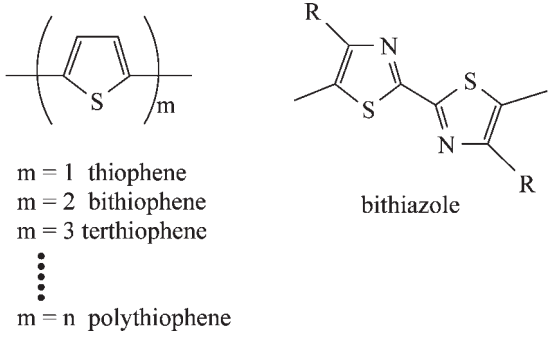

Figure 1. Structures of oligothiophene and bithiazole.

functional materials.[3,4,8] With these concepts in mind, my research group is actively involved in developing versatile synthetic routes to a new range of alkyne-functionalized α-coupled thiophene oligomers at their end positions, which can then provide direct access to various metallated materials bearing these π-conjugated systems. The introduction of transition metal centers, with their large variety of ligand environments and oxidation states, can lead to interesting physical properties on the oligothiophene systems. Especially, π-conjugation of organometallic moieties into the oligothiophene chain should provide interesting models that possess unique properties which are not observed in the organic counterparts.[9] In this review, such oligothiophene-derived metallayne systems are surveyed and the roles of metals on their photophysical and structural properties are discussed. In several occasions, the bithiazole unit was also employed and the results were compared to those for the corresponding bithiophene counterparts (Figure 1). It is known that poly(thiophene-2,5-diyl) and its derivatives are composed of "electron-excessive" heterocyclic units (*p*-doping) whereas polymers such as poly(pyridine-2,5-diyl) contain "electron-withdrawing" imine nitrogen (*n*-doping).[10] It is conceived that incorporation of a thiazole ring, a hybrid of the thiophene and pyridine groups, in the main chain of the organometallic systems is attractive as a new approach for the control of energy gap.

2. SYNTHESIS OF DIETHYNYL-BASED OLIGOTHIOPHENES AND BITHIAZOLES

The TMS-functionalized oligothiophene precursors **Ia**–**Ic** were prepared by a Pd^{II}/CuI-catalyzed cross-coupling reaction of the corresponding dibromides with trimethylsilylacetylene (Scheme 1).[11] These ligands are all stable in air and toward light. 4,4′-Di(*tert*-butyl)-2,2′-bithiazole was synthesized by the reaction of 1-bromopinacolone and dithiooxamide in refluxing ethanol.[12,13] Starting with 2-bromo-4′-methoxyacetophenone, 4,4′-di(*p*-methoxyphenylene)-2,2′-bithiazole can similarly be made.[13] The dibromobithiazoles can then be obtained by direct bromination with Br_2, which can then furnish the TMS-protected compounds **Id** and **Ie** as yellow solids. Conversion of **Ia**–**Ie** into **IIa**–**IIe** was accomplished by the desilylation of **Ia**–**Ie** with K_2CO_3 in MeOH. While the terminal acetylenes **IIa**–**IIc** are not stable in solution or on exposure to light for long periods and give insoluble brown precipitates on

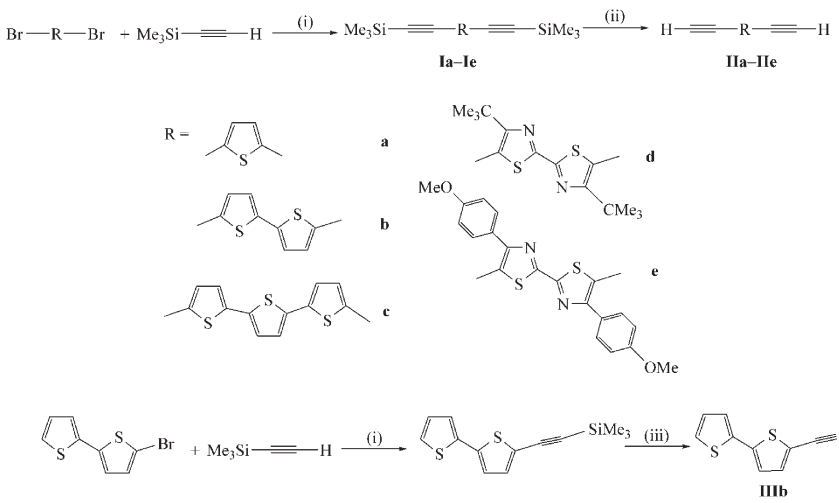

Scheme 1. Synthesis of diethynyl-based oligothiophenes and bithiazoles. (i) $Pd(OAc)_2$, PPh_3, CuI, $^iPr_2NH$; (ii) K_2CO_3, MeOH; (iii) KOH, MeOH.

standing, the ligands **IId** and **IIe** are solids of high air stability. 5-(Trimethylsilylethynyl)-2,2′-bithiophene was prepared from 5-bromo-2,2′-bithiophene and this ligand can be proto-desilylated to give **IIIb** using methanolic KOH.[14]

3. PLATINUM(II) ACETYLIDES

The platinum(II) model compounds **1a–1d** and polymers **2a–2d** were prepared by the dehydrohalogenation reactions (Scheme 2).[11,12,15,16] Treatment of **IIa–IId** with two molar equivalents of *trans*-$[PtPh(Cl)(PEt_3)_2]$ in $CH_2Cl_2/^iPr_2NH$, in the presence of CuI, produced **1a–1d**, after TLC purification on silica. Likewise, the CuI-catalyzed reaction between *trans*-$[Pt(PBu_3)_2Cl_2]$ and **IIa–IId**, in a 1:1 molar ratio, in $^iPr_2NH$, readily provided soluble polymers **2a–2d**. Purification of **2a–2d** was accomplished by alumina column chromatography using CH_2Cl_2 as eluent and they were each isolated in high purity after repeated precipitation from a toluene/MeOH mixture. The molecular weights of the polymers were determined by GPC in THF. The weight-average molecular weight (M_W) value ranges from 47500 to 219940 and indicate a high degree of polymerization. The thermal properties of the polymers were also studied by TGA and DSC (Table 1).

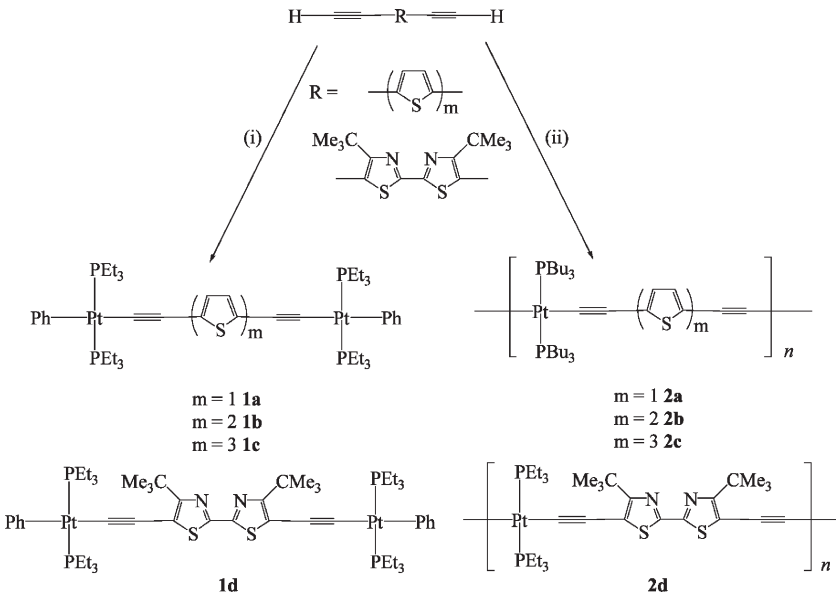

Scheme 2. Synthesis of compounds 1a–1d and 2a–2d. (i) *trans*-[Pt(PEt$_3$)$_2$PhCl], ^{i}Pr$_2$NH, CuI; (ii) *trans*-[Pt(PBu$_3$)$_2$Cl$_2$], ^{i}Pr$_2$NH, CuI.

Compounds **1a–1d** and **2a–2d** have been fully characterized by elemental analyses, mass spectrometry, IR and NMR spectroscopies. The structures of **1a**, **1b** and **1d** were ascertained by X-ray crystallography.[11,12] In each case, the crystal structure consists of discrete dimeric molecules in which the platinum atoms are surrounded by four ligands in a square planar geometry with the two phosphines in a *trans* disposition. For **1b** and **1d**, there are two independent half molecules each possessing crystallographic C_i symmetry (Figures 2 and 3). The

Table 1. Structural and thermal properties of the polymers

Polymer	Yield/%	M_w^a	M_n^a	T_{decomp}/°C	T_g/°C
2a	87	219940	*b*	*b*	*b*
2b	65	181900	56180	278 ± 8	275
2c	61	82860	64560	290 ± 15	281
2d	60	47500	40390	321 ± 8	215

[a]GPC against polystyrene calibration.
[b]Not reported.

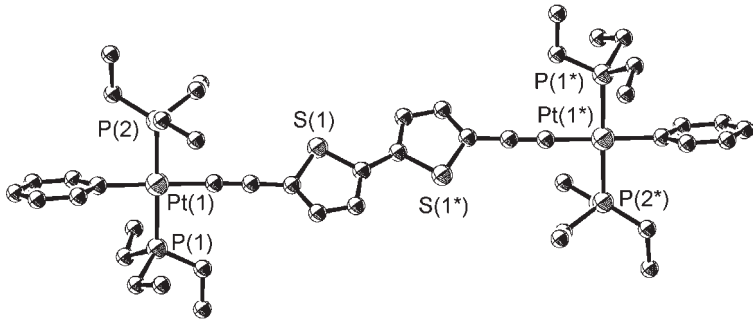

Figure 2. Molecular structure of **1b**.

metal-to-phosphorus bond lengths lie in the range of 2.274(5)–2.303(5) **(1a)**, 2.291(6)–2.316(6) A **(1b)** and 2.295(3)–2.297(3) A **(1d)**. The two five-membered rings in **1b** and **1d** display a *trans* arrangement in order to minimize the steric repulsions between the lone pairs on both sulfur atoms. The mean Pt−C(alkyne) bond length is 2.03(2) Å **(1a)**, 2.01(2) **(1b)** and 2.001(9) Å **(1d)**, while the average acetylide C≡C bond length is 1.20(3) **(1a)**, 1.25(3) **(1b)** and 1.22(1) Å **(1d)**.

The electronic absorption spectra of **IIa–IIc** show strong, relatively low-energy π–π^* transitions (Table 2). An increase of the number of thienyl units, m, in the molecule shifts the position of these bands toward longer wavelengths. Presumably, a higher degree of conjugation with the additional thienyl units reduces the energy gap between the highest occupied and lowest unoccupied molecular orbitals (HOMO and LUMO). This is consistent with the π–π^* transition observed for the parent oligothiophenes, which vary from 231 nm for thiophene to 350 nm for terthiophene.[17] For **IIa–IIc**, the lowest energy transition

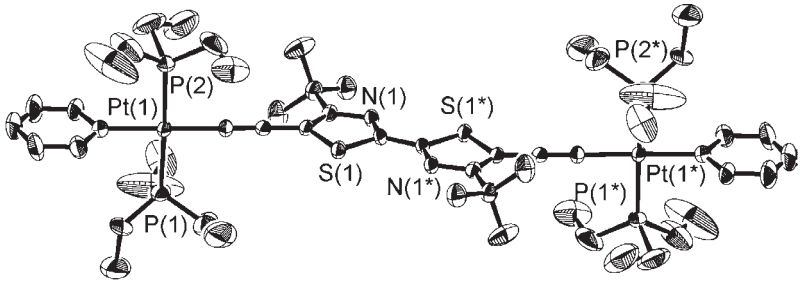

Figure 3. Molecular structure of **1d**.

Table 2. Absorption and emission data for the diethynyl ligand precursors

Ligand	Absorption λ_{max}/nm ($\varepsilon/10^4\ M^{-1}\ cm^{-1}$)[a]	Emission λ_{em}/nm(Φ)[a]
IIa	293 (0.06), 305sh (0.06)	359 (0.019)
IIb	344sh (0.2), 355 (2.2)	392sh, 411 (0.058)
IIc	393 (2.4)	444, 467sh (0.086)
IId	372 (2.5)	414sh, 431 (0.066)
IIe	290 (5.5), 399 (1.6)	465 (0.024)
IIIb	333 (2.2)	392[b]

[a]In CH_2Cl_2.
[b]Φ was not reported. sh = shoulder.

red-shifts steadily from 305 to 393 nm. As far as the absorption data of the Pt(II) complexes are concerned, the following trends are observed (Table 3): (i) The energy of the optical gap of the polymers decreases with an increase in the value of m. We attribute this to an increased delocalization of π-electrons along the polymer chain. As the m value increases, the overall effect on the band gap decreases, and there would probably be little benefit in increasing the number of thiophene units above three. (ii) Attaching a Pt fragment at each end of the ligands lowers the energies of the transition. In the same way, the transition energies of the polymers are lowered compared to the corresponding monomers, in line with π-conjugation of the ligands into and through the metal center.

Figure 4 depicts the room temperature photoluminescence (PL) spectra for polymers **2a–2c**. The emission features are shifted to lower energy with the increasing length of the thiophene segment, reminiscent

Table 3. Absorption data and optical gaps for platinum(II) complexes and polymers

Compound	λ_{max} in CH_2Cl_2/nm	λ_{max} in CH_2Cl_2/eV	Optical gap/eV[a]
1a	378	3.28	[b]
1b	406	3.05	[b]
1c	433	2.86	[b]
1d	432, 454sh	2.73, 2.87	2.55
2a	416	2.98	2.80
2b	458	2.71	2.55
2c	470	2.64	2.40
2d	439sh, 464	2.67, 2.82	2.35

[a]Estimated from the absorption edge.
[b]Not reported.

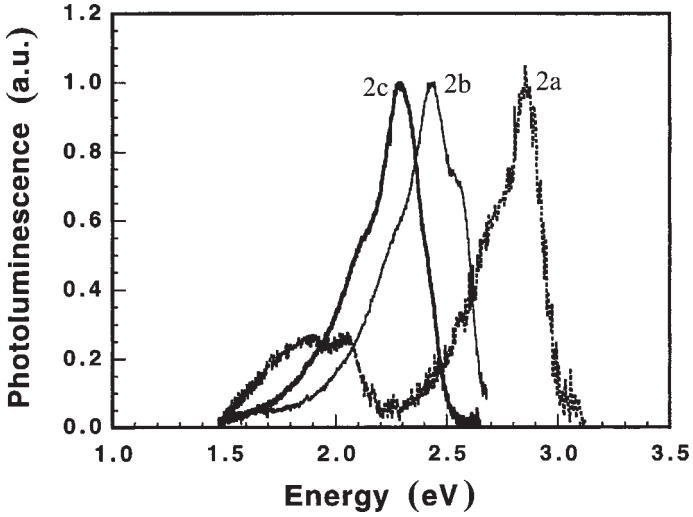

Figure 4. Photoluminescence spectra of **2a–2c**.

of the absorption spectra. We attribute the peaks at 2.85, 2.44, 2.28 eV for **2a–2c**, respectively, to emission from the singlet excited state (fluorescence), due to the small Stokes shift between absorption and emission features. We note that the singlet S_0–S_1 transition involves the mixed ligand–metal orbitals, dominated either by the intraligand HOMO–LUMO π–π^* transition or charge-transfer type transition. The broad feature between 1.6 and 2.2 eV in the PL spectrum of **2a** arises from a triplet state emission (phosphorescence) due to strong spin-orbit coupling induced by the heavy metal centers that allows for an efficient intersystem crossing (ISC). We identify the emission peak at 2.05 eV in 2a as a triplet emission for the following reasons: First, this emission is strongly temperature dependent in contrast to the singlet emission (Figure 5). From 180 K to 16 K, the singlet emission peak increases by a factor of 2.4, while the lower-lying emission increases by a factor of 19.4. This increase of emission intensity indicates a long-lived excited state that is quenched by thermally activated diffusion to dissociation sites. Second, for similar systems such as *trans*-[$-Pt(PBu_3)_2-C\equiv C-p-C_6H_4-C\equiv C-]_n$, we also found a higher-lying singlet emission (at 3.2 eV) and a lower-lying, clearly identified triplet emission (at 2.4 eV).[18] The latter is also increased by a factor of about 20 when going from 180 K to 20 K and was found to have a lifetime of 30 μs at 10 K.[19]

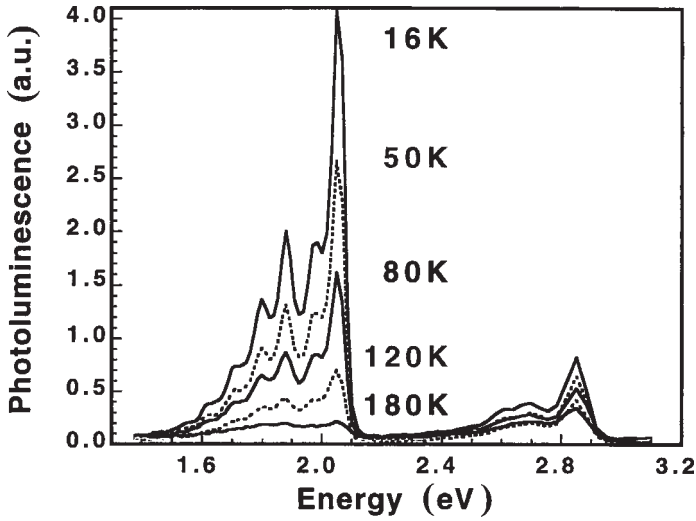

Figure 5. Temperature dependence of the photoluminescence of **2a**.

For **2b**, there is a weak triplet emission shoulder centered at about 1.67 eV. There is no room temperature triplet emission for **2c** over the measured range (1.2–3.0 eV). At 18 K, triplet emissive peaks become more apparent at 2.05, 1.67 and 1.53 eV for **2a–2c**, respectively, and they all energetically lie at 0.80–0.88 eV below the singlet emission (Figure 6). We observe two key points here: (i) The intensity of this triplet emission decreases rapidly with increasing number of thiophene units. Two factors can account for this observation. First, the higher m value in the ligand reduces the influence of the heavy metal center which is mainly responsible for ISC. Next, in oligothiophene systems themselves, ISC is reduced with increasing value of m, as the energy of the singlet excited state drops below the corresponding resonance state for ISC in those systems.[20] (ii) The energy of the triplet emission shifts (Figure 6) when adding more thiophene rings in the ligand (from 2.05 eV to 1.53 eV for **2a–2c**, $\Delta E = 0.52$ eV). This indicates that the triplet excited state should be extended over several thiophene rings (i.e three or more) in the present systems where we increase the conjugation length within the ligand. This is in contrast to the similar position ($\Delta E \leq 0.03$ eV) of the triplet emission in polymers and corresponding monomers of *trans*-$[-Pt(PBu_3)_2-C\equiv C-R-C\equiv C-]_n$ ($R = C_6H_4$, C_5H_3N).[16b] This shift of triplet emission energy observed in **2a–2c** also agrees with the

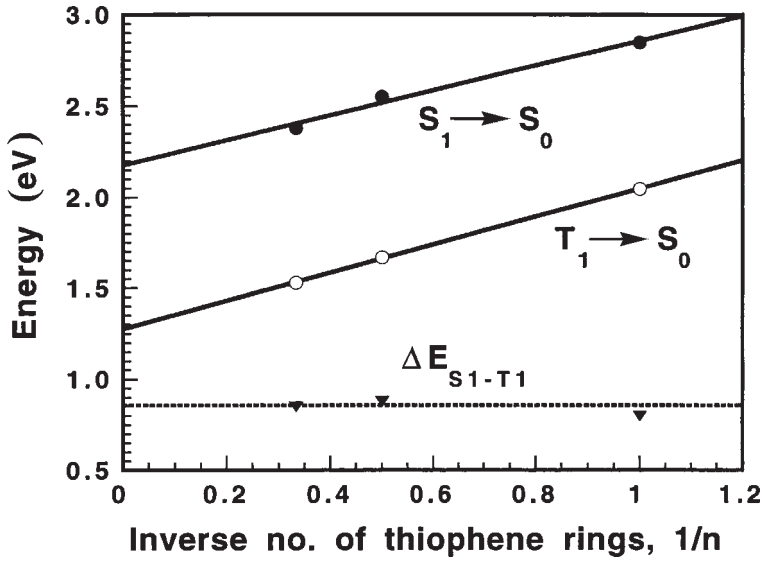

Figure 6. Evolution of the $S_1 - S_0$ and $T_1 - S_0$ excitation energies, and the singlet–triplet energy gaps $\Delta E_{S_1-T_1}$ with the inverse number of thiophene rings (1/n) in the bridging ligand.

calculations by Beljonne et al. on the evolution of the triplet excitation energy in purely organic oligothiophene systems.[20,21]

The photocurrent action spectra of **2a–2c** were also studied and Figure 7 shows the photocurrent quantum yields as a function of the photon energy in short-circuit mode for illumination through the ITO or gold electrode for **2a–2c**. The photocurrent spectra of the Au/**2a**/Al, ITO/**2b**/Al and ITO/**2c**/Al photocells show two peaks, one at the onset of absorption [2.92 (**2a**), 2.64 (**2b**) and 2.43 eV (**2c**)] and one at higher photon energies [3.81 (**2a**), 3.56 (**2b**) and 3.38 eV (**2c**)]. This is consistent with the UV photocurrent spectra reported for poly(*p*-phenylenevinylene)[22] and for Pt(II) polyyne containing a thienopyrazine ring.[23] We tentatively interpret the second photocurrent peaks as caused by absorption into the higher-lying absorption bands. The position of the first photocurrent peak at the onset of absorption is determined by factors such as the internal filter effect[24] and increased charge separation at low energy sites.[25] Polymers **2a–2c** show a short-circuit quantum efficiency of about 0.04% at the first photocurrent peak, which is a common value for single-layer devices. There is no great difference in quantum efficiency with variation of the thiophene content in

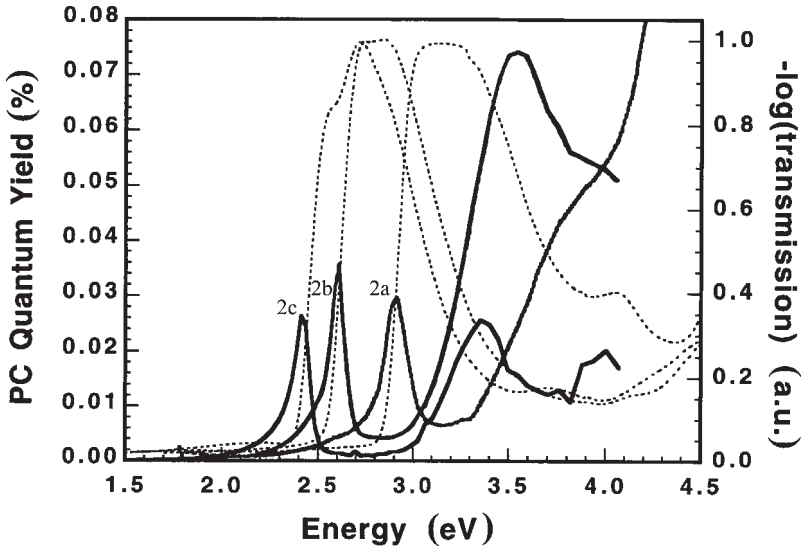

Figure 7. Photocurrent spectra of the photocells Au/**2a**/Al, ITO/**2b**/Al and ITO/**2c**/Al. Absorption spectra (···) are also shown for comparison.

the polymer. The quantum efficiency of the second peak is different for **2a**, **2b** and **2c** and is very sensitive to air exposure. The overall photocurrent increases when exposed to air and is reduced after annealing under vacuum. The current-voltage characteristics taken under illumination at intensities of 90, 185 and 440 $\mu W/cm^2$ at the first peak in the spectral response give open-circuit voltages of 0.50, 0.75 and 0.47 and fill-factors of 0.32, 0.35 and 0.30 for **2a**–**2c**, respectively. These are typical values for single-layer polymeric photocells.

The spectrum of **1d** is dominated by the $\pi-\pi^*$ bands of the bridging ligand, and coordination of Pt(II) groups to the termini lowers the transition energy. The spectral features of polymer **2d** resemble those of the model compound **1d** but their transition energies are reduced. In each case, the absorption peaks show a significant red-shift compared to their bithienyl counterparts due to the presence of the electron-withdrawing imine nitrogen atoms. As compared to poly(alkylbithiazole)s,[10] the absorption maxima also shift to longer wavelengths upon incorporation of heavy Pt(II) groups in the polymer backbone. We also note the optical gap order as 2.78 (**IId**) > 2.55 (**1d**) > 2.35 eV (**2d**), and the bandgap of **2d** is smaller than that in **2b** by 0.2 eV. Thin films of **1d** and **2d** show the

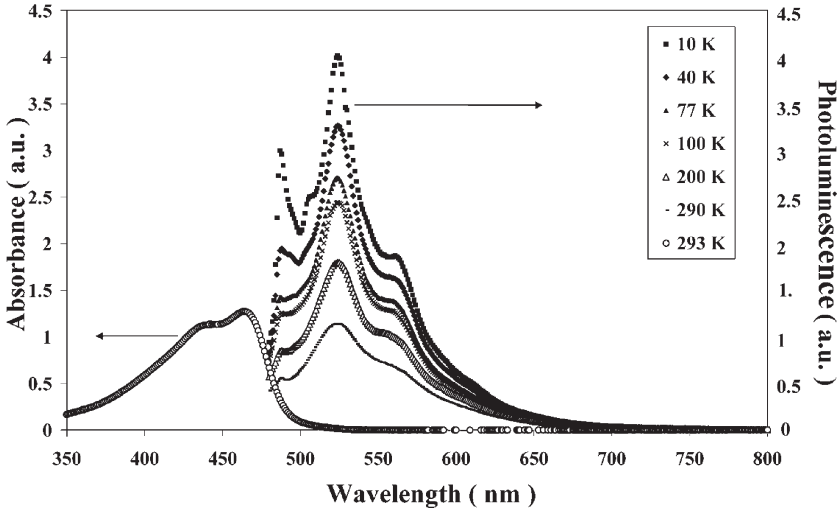

Figure 8. Absorption and variable temperature emission spectra of **2d**.

PL bands at 537 **(1d)** and 539 nm **(2d)** at room temperature. Like **2a–2c**, we attribute this peak to emission from singlet excited state ($S_1 \rightarrow S_o$) due to the small energy shift (*ca.* 0.35 eV) between the strongest bands in the absorption and emission spectra. This assignment is also consistent with the observed temperature dependence of the emission features for **2d** (Figure 8). From 290 K to 10 K, the singlet emission peak only increases by a factor of 3.2, suggesting a rather short-lived excited state. For **2d**, another electronic transition at 562 nm at 10 K emerges from the evolution of the vibronic sidepeaks with temperature. This peak shifts slightly to lower energy with decreasing temperature in contrast to the other peaks. Similar to *trans*-[$-Pt(PBu_3)_2$-C≡C-p-C_6H_4-C≡C$-]_n$, this emission feature was attributed to the phosphorescence signal by interchain interaction.[26] As the temperature increases, the vibronic substructure located at about 487 nm gradually disappears, analogous to that observed in **2b**.[16a]

4. GOLD(I) ACETYLIDES

There has been much interest in gold(I) σ-acetylide complexes and related polymers, which is not only due to their remarkable luminescent properties,[27] but also to the possibility that they may exhibit novel electrical conducting and nonlinear optical behavior.[28] The initial

studies that confirmed that gold(I) σ-acetylides represented a new class of luminophores were carried out on $[Au_2(\mu\text{-dppe})(C{\equiv}CPh)_2]$.[29] An X-ray crystal structure of this complex suggested an intermolecular Au···Au interaction of 3.152(2) Å that holds two complexes together in a *transoid* configuration to form a dimer. It was clearly shown that the presence of the Au···Au interaction is key to the luminescent properties of the compound. Since then, a plethora of studies have been undertaken. These alkynylgold(I) phosphine complexes exhibit rich luminescent behavior with long-lived excited states. The origin of the emission is strongly dependent on the nature of the phosphine ligands and the acetylide units. From the reported solid-state structures of gold(I) σ-acetylides, a study of the L–Au–C≡CR (L = phosphine, R = aryl group) fragments shows that Au–L, Au–C and C≡C bond lengths vary in a narrow range irrespective of the changes in L and R. The molecular shape seems mostly governed by the aryl group(s) in the acetylide ligand. However, the complementary intermolecular forces of Au···Au interactions, hydrogen bonding, $\pi-\pi$ stacking and other non-covalent interactions combine to produce novel dimers, oligomers, chains and 2-D networks. In many cases, it is the combination of these interactions that determines the solid state luminescent properties of these materials. Following the studies on optoelectronically active platinum polyyne complexes and polymers, we further our investigations on a series of gold(I) complexes with the acetylide-functionalized thiophenes.

A series of stable mono- and digold alkynyl complexes were synthesized from the reaction of the freshly prepared alkyne **IIa–IIc** and **IIIb** with a stoichiometric quantity of the gold(I) phosphine chloride in CH_2Cl_2 at room temperature in the presence of NaOMe in MeOH (Scheme 3).[14]

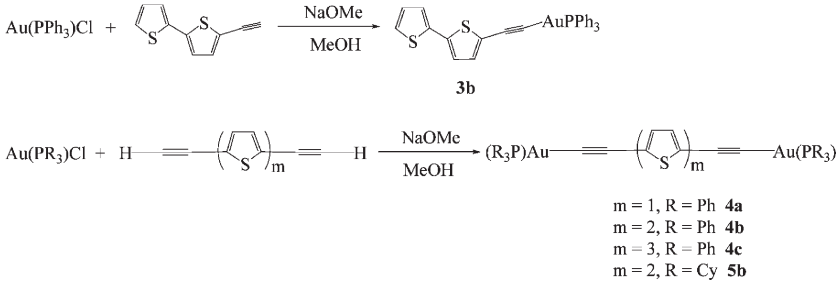

Scheme 3. Synthesis of some gold (I) alkynyl complexes with oligothienyl units.

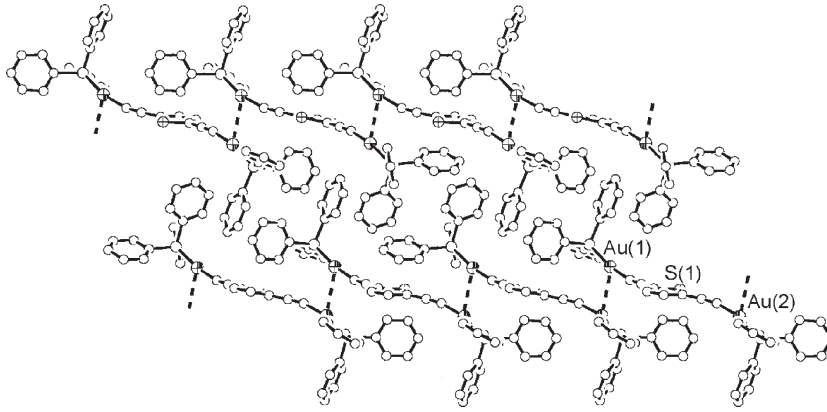

Figure 9. Packing diagram of **4a**, showing the intermolecular Au · · · Au interactions.

They were characterized by spectroscopic and crystallographic methods. Crystal structure analyses show that for the digold system with one thiophene group **4a** (Figure 9), a loose polymeric structure is formed through aurophilic Au · · · Au interactions (3.2915(10) and 3.2347(9) Å). The asymmetric unit in **4a** contains two molecular units, and the Au · · · Au interactive {(Ph_3P)AuC≡C−} vector is *anti*-parallel with a torsion angle (−C≡C−Au · · · Au−C≡C−) of 172.2°. However, for the mono-gold complex **3b**, intermolecular Au · · · S and $\pi \cdots \pi$ interactions are dominant, and for **4b**, **4c** and **5b**, neither Au · · · Au or Au · · · S intermolecular interactions are observed. Figures 10 and 11 depict perspective views of **4b** and **4c**, respectively. It seems that as the linker group between the gold centers in acetylene-functionalized complexes becomes longer, the possibility of oligomer or polymer formation through non-covalent intermolecular

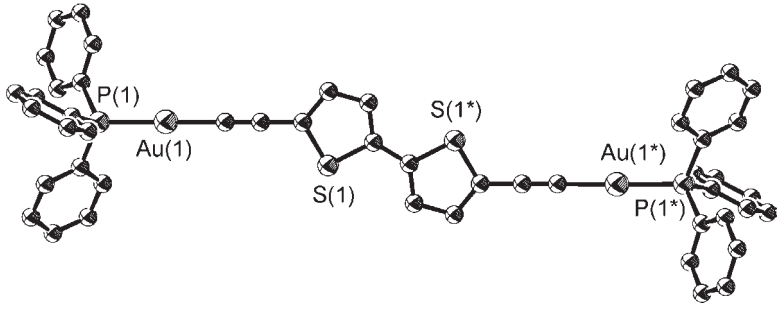

Figure 10. Molecular structure of **4b**.

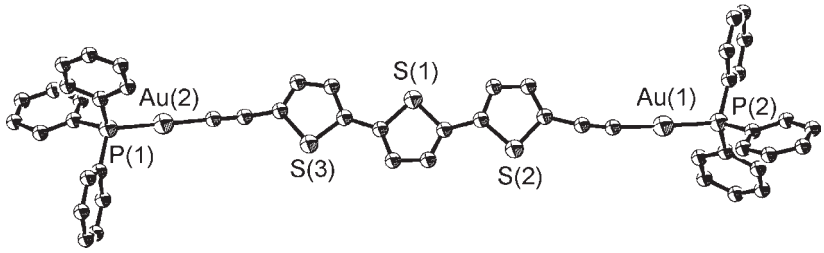

Figure 11. Molecular structure of **4c**.

interactions significantly decreases. Thus, the formation of polymeric gold acetylide systems through Au···Au interactions is highly dependent on the length and steric properties of the acetylene-functionalized spacer group, and is seemingly restricted to complexes with only one ring between the two acetylenic units in the digold systems. By comparison, the related platinum complexes **2a**–**2c** do not display any significant intermolecular interactions, regardless of the value of m. This probably reflects the increase in steric shielding around the core of the molecule caused by the presence of two bulky phosphine ligands around each square planar Pt(II) center.

In general, these gold(I) complexes absorb strongly in the range 290–450 nm (Table 4), and the peak shape of the complex is similar to that of its parent acetylide ligand, but the peak maxima are shifted to longer wavelengths. The strong dependence of the absorption spectra on the nature of the acetylide ligands suggests that the transitions are $\pi-\pi^*$ ligand centered and the insensitivity of the low energy absorption bands toward the anxiliary ligands on the gold center (*cf.* **4b** *vs.* **5b**) precludes an Au(I)-centered origin for these transitions. However, the red-shift of the spectra in the complexes indicates π-interaction of the

Table 4. Absorption and emission data for gold(I) alkynyl complexes

Compound	Absorption λ_{max}/nm ($\varepsilon/10^4 M^{-1}cm^{-1}$)	Emission λ_{em}/nm (relative intensity[a])
3b	354 (3.2), 380sh (1.7)	393 (0.88), 411 (1)
4a	339 (6.0), 361 (6.9)	374 (0.86), 390 (1)
4b	373sh (4.8), 391 (5.4), 415sh (3.6)	432 (1), 455 (0.98), 495sh (0.34)
4c	401sh (5.5), 421 (6.0), 451sh (3.5)	472 (1), 499 (0.80), 545sh (0.26)
5b	370sh (4.2), 390 (5.0), 414sh (3.3)	430 (1), 453 (0.95), 495sh (0.33)

[a]Intensity of the strongest peak is assigned as unity.

gold centers with the acetylide bridges. Therefore, the spectra are likely to be dominated by ligand $\pi-\pi^*$ transitions, but mixed with a small contribution from σ(Au−C) in the HOMO and some Au $6p_\pi$ in the LUMO.[30] Although the possibility of a MLCT origin for these absorptions cannot be ruled out totally, it must be of minor importance, since the absorption and emission spectra for **4a** in the less polar solvent, toluene (λ_{abs}342, 366 nm; λ_{em}378, 394 nm) showed insignificant differences from those in CH_2Cl_2. However, it should be noted that the spectra were measured in solution where $Au(I)\cdots Au(I)$ interactions are likely to be less significant, particularly for **4a**.

The increase in λ_{max} ($\Delta\lambda_{max}$: 21 nm for **3b** *vs.* **IIIb**) upon introducing one $[Au(PPh_3)]^+$ unit onto a mono-acetylene ligand, is about half the value after the introduction of two $Au(PPh_3)$ units onto the corresponding diacetylene ligand ($\Delta\lambda_{max}$: 36 nm for **4b** *vs.* **IIb**). Similarly, the change in the absorbance maxima is also about half the value. As the number of bridging aromatic rings increases, there is a sequential increase in the absorption maxima; however, the value of the red-shift associated with the coordination of the gold(I) fragment decreases, *i.e.* in going from **4a** to **4b** to **4c**. This is consistent with the gold-centered orbitals contributing less to the HOMO and LUMO levels as the number of rings increases, and hence π-conjugation increases.

The gold(I) complexes show emission maxima that follow the same trend as their absorption maxima. There is little change in the emission spectra upon variation in the excitation wavelength indicating that a single emissive state or multiple states in equilibrium is(are) responsible for the observed emission. The emission maxima are dependent on the nature of the acetylide ligand and thus the lowest emissive states in the complexes can tentatively be assigned as gold-perturbed $^1(\pi-\pi^*)$ transitions. The relative intensity of the higher energy peak in the emission spectrum of **4a**–**4c** increases in moving from the monothiophene to the terthiophene. The average change per bond from the geometric relaxation upon excitation diminishes as the number of linking rings increases, which results in the higher intensity of a transition to the lower vibronic states, in accordance with the Franck-Condon principle.[31]

5. MERCURY(II) ACETYLIDES

Studies of weak intermolecular d^{10}-d^{10} $Au\cdots Au$ bonding interactions in gold(I) systems and how these can influence conformations, crystal

packing and chemical transformations represent a challenging area of research. In contrast to the extensive body of work on discrete and polymeric alkynylgold(I) species, related studies on the isoelectronic mercury(II) system remain relatively unexplored. To our knowledge, studies of binuclear alkynylmercury(II) complexes are very rare. Based on the isolobal analogy between $[Au(PPh_3)]^+$ and $[HgR]^+$ (R = Me, Ph) fragments,[32] a comparative investigation of the alkynylmercury(II) complexes to their gold(I) congeners will be a valuable addition to this important area of research. We have studied a series of bis(alkynyl) mercury(II) complexes with oligothiophene and bithiazole linking units.[33]

Following the classical dehydrohalogenating route, treatment of two equivalents of MeHgCl or PhHgCl with each of **IIa–IIe** in an excess of NaOMe in MeOH readily provided the dimercury(II) diacetylide complexes **6a–6e** and **7a–7e** in very good yields (Scheme 4). The reaction is complete after stirring at room temperature for 15 h and the products can be precipitated from the solution mixture. All these new compounds were isolated as air-stable yellow to orange solids in high purity and exhibit fairly good solubility in chlorinated solvents such as CH_2Cl_2 and $CHCl_3$.

For **6a** and **6b**, the crystal structures consist of discrete dimeric molecules in which the mercury centers adopt a two-coordinate linear geometry to afford the expected rod-like skeleton. Reminiscent of the PAuC≡C unit in the analogous Au(I) complexes, the isoelectronic MeHgC≡C fragment displays similar structural motifs in **6a** and **6b**. The Hg−C(alkyne) bonds (2.036(13) and 2.042(13) Å **6a**; 2.02(2) and 2.05(2) Å **6b**) are slightly longer than the Au−C(alkyne) bonds in the isostructural Au(I) complexes (1.997(6) and 2.005(6) Å **4a**; 2.004(4) Å **4b**) but comparable to those in other Hg(II) acetylide compounds.[33,34] The C≡C bond lengths in the ethynyl bridge are fairly typical of metal acetylide σ-bonding (1.196(18), 1.202(18) Å for **6a**; 1.22(3), 1.26(3) Å for **6b**). For **6b**, the two thiophene rings exhibit *anti*-configuration to minimize the repulsion between the β-hydrogens on the adjacent rings. Both structures revealed the presence of weak intermolecular noncovalent Hg···Hg interactions (3.777, 3.935 Å for **6a**, 3.851 Å for **6b**), which link the molecular units together to form a loose polymeric structure. For **6a**, the lattice is stabilized through extensive Hg···Hg interactive vectors in a 3-D arrangement (Figure 12) and the closest intermolecular nonbonded Hg···S contact is due to the Hg(2)···S(1) interaction (4.072 Å). There are also short contacts involving the thienyl

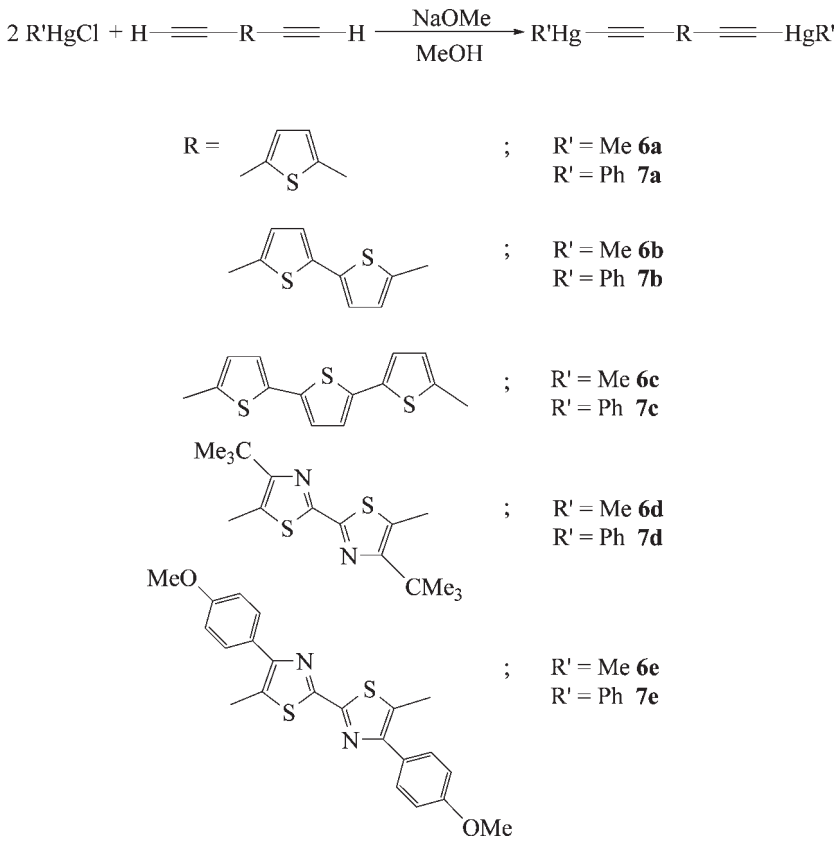

Scheme 4. Synthesis of compounds 6a–6e and 7a–7e.

sulfur and methyl hydrogen atoms (2.999 and 2.952 Å). An inspection of the crystal packing diagram of **6b** (Figure 13) shows a large dihedral angle (*ca.* 26.7°) between the two thiophene planes. We also observe a short contact between Hg(1) and S(2) (3.752 Å), which is probably caused by the donation of electron density from the sulfur lone pair to an empty hybrid orbital on the mercury. The lattice structure is highlighted by the presence of weak Hg · · · Hg interactions in a 2-D network.

All the Hg(II) complexes exhibit rich absorption and luminescence behavior as a function of the number of thiophene rings as well as the electronic nature of the five-membered rings within the bridging ligand (Table 5). In general, the absorption spectra of the Hg(II) complexes display intense bands in the range 297–438 nm, and the peak maxima are

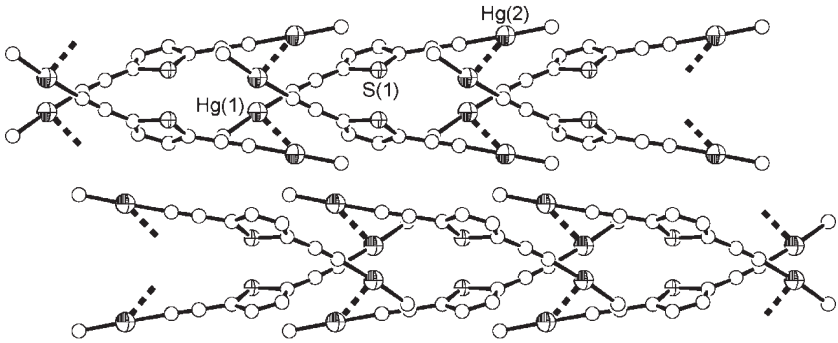

Figure 12. Packing diagram of **6a**, showing the intermolecular Hg · · · Hg interactions.

shifted to longer wavelengths as compared to those of the free alkynes. The strong dependence of the solution absorption spectra on the nature of the central linker unit suggests the absorption peaks to arise from ligand-localized $\pi-\pi^*$ transitions, and the apparent insensitivity of these bands toward the hydrocarbyl group R′ on Hg (*cf.* **6b** *vs.* **7b**) precludes a Hg(II)-centered origin for these transitions. However, the absorption features show bathochromic shifts when the terminal Hg(II) units are introduced, and such a red-shift reveals π-delocalization through the Hg(II) centers due to metal to ligand back-donation to π^*(C≡CR). Based on the observed data, the spectra are probably dominated by

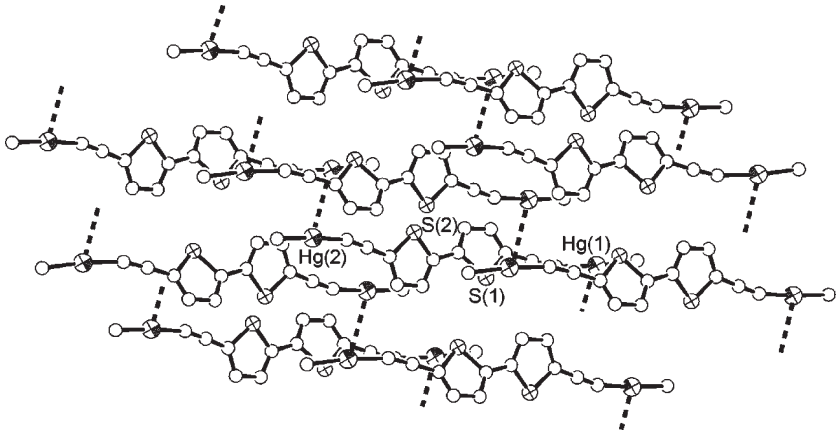

Figure 13. Packing diagram of **6b**, showing the intermolecular Hg · · · Hg interactions.

Table 5. Electronic absorption and emission data for the mercury(II) alkynyl complexes

Compound	λ_{max}/nm (ε/10^4 M^{-1} cm^{-1})[a]	λ_{em}/nm (Φ)[a]
6a	318 (2.5), 337 (2.5)	361 (0.007)
6b	348 (2.6), 368 (2.6), 384 (2.3)	409 (0.025)
6c	412 (3.0)	461, 490sh (0.067)
6d	393 (3.9), 414sh (2.5)	460, 488sh (0.050)
6e	297 (4.8), 413 (2.5), 430sh (2.3)	470 (0.016)
7a	323 (0.4), 341 (0.3)	361sh, 394 (0.006)
7b	348 (2.4), 368 (2.8), 384 (2.4)	417sh, 439 (0.020)
7c	412 (2.8)	464, 494sh (0.069)
7d	393 (4.3), 414sh (0.3)	435, 458 (0.043)
7e	299 (4.8), 414 (2.8), 438sh (0.2)	468 (0.014)

[a]In CH_2Cl_2. sh = shoulder.

ligand-based $\pi-\pi^*$ transitions, but mixed with a small contribution from the metal in the HOMO and the LUMO. This agrees well with the molecular orbital calculations on **6a** and **6b**. Figure 14 depicts the contour plots of the HOMO and LUMO for **6a** and **6b**. The calculated HOMO–LUMO gap follows the order **6a** (4.19 eV) > **6b** (3.76 eV), in line with our experimental observations. The metal contributions based on the Mulliken population analysis[35] to the HOMO and LUMO are small in both cases (HOMO 3.0, LUMO 20.0% from each Hg for **6a**; HOMO 1.5, LUMO 7.0% from each Hg for **6b**).

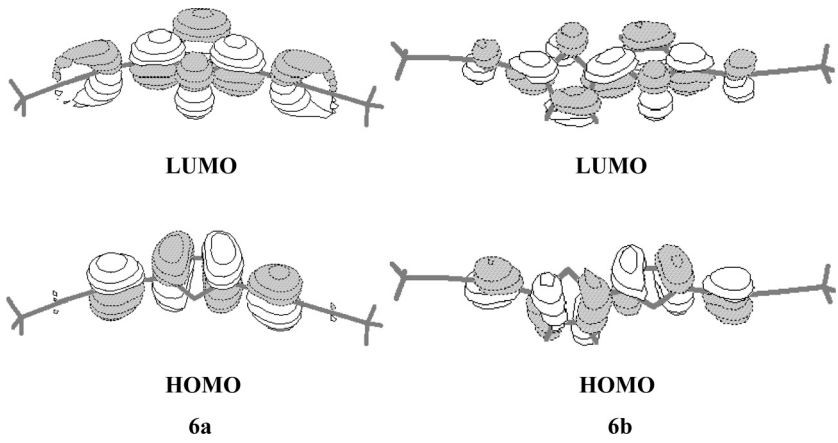

Figure 14. Contour plots of the HOMO and LUMO for **6a** and **6b**.

The introduction of the Hg(II) moiety is found to lower the transition energies and to increase the absorption intensity, indicating an enhancement in the degree of π-delocalization through the mercury conjugated system, but the extent of the red-shift is smaller as compared to that imparted by the $[AuPPh_3]^+$ moiety (e.g. 293 **IIa**, 337 **6a**, 361 nm **4a**). The more marked effect for Au(I) is consistent with the lower oxidation state of +1 in gold(I) complexes, which would enhance the back-donation to π^*. Increasing conjugation through more thienyl rings leads to a decreased transition energy and an increase in the molar absorption coefficients for **6a**–**6c** as well as **7a**–**7c**. Thus, a red-shift of *ca*. 75 nm is observed from **6a** to **6c**, whereas the shift is 71 nm from **7a** to **7c**. However, the value of the red-shift induced by the end substitution of Hg(II) groups decreases with increasing m. These results are also consistent with the mercury-based orbitals contributing less to the HOMO and LUMO levels as the number of thiophene rings increases and hence π-conjugation increases. Replacing the bithiophene spacer in **6b** by a bithiazole moiety in **6d** and **6e** notably lowers the HOMO−LUMO gap, suggestive of enhanced conjugation in the latter. The bathochromic shift of 10–20 nm compared to their bithienyl counterparts can be ascribed to the unique electron-withdrawing imine nitrogen atoms in the bithiazole derivatives.[10] The absorption peak of **6e** (or **7e**) is also red-shifted relative to **6d** (or **7d**), by virtue of the increased π-conjugation through the *p*-methoxyphenyl group in the former case.

The emission maxima of **6** and **7** roughly follow the same order as the absorption energies. The emission energy varies with the nature of R (Figure 15) but does not change much with R′. Their similar spectral patterns as their free alkynes are suggestive of the ligand-dominating emissive state and the lowest emissive states in these complexes can tentatively be assigned as metal-perturbed $\pi-\pi^*$ transitions. With increasing thiophene content, the emission features are both red-shifted and the emission quantum yields are increased. The orders of emission energies **6a** > **6b** > **6c** and **7a** > **7b** > **7c** are observed in moving from the monothiophene to the terthiophene. We can possibly attribute the quenching in the luminescence intensity to the heavy-atom effect which catalyzes the non-radiative deactivation of the excited states of the fluorophore.[36] Due to the lack of available low-lying metal-localized excited states, it is unlikely that energy or electron transfer quenching mechanism operates here. The emission spectra for the bithiazole derivatives also show a significant red-shift as compared to their bithienyl counterparts.

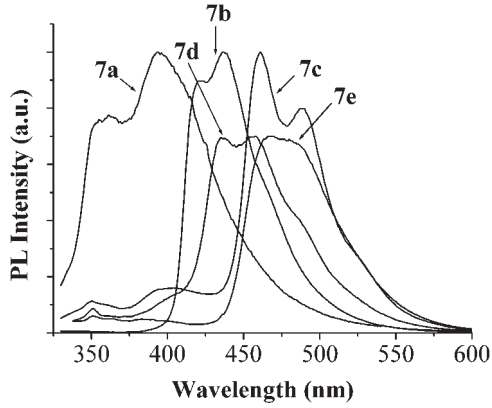

Figure 15. Emission spectra of **7a–7e** in CH_2Cl_2 at 293 K.

6. COBALT CARBONYL ALKYNE COMPLEXES

The synthetic approach can also be extended to the cobalt system based on the well-known coordination of C≡C triple bond toward $Co_2(CO)_6$ core in an η^2-fashion.[37] The cobalt carbonyl derivatives [{$Co_2(CO)_6$}$_2$-(diyne)] **8b** and **9b** were prepared from the reactions of two molar equivalents of [$Co_2(CO)_8$] with the appropriate diynes in *n*-hexane at 0°C (Scheme 5).[38] They are not air-sensitive in the solid form but slowly decompose to uncharacterized black materials in solution in several days. The molecular structure of **9b** is illustrated in Figure 16. The crystal structure shows that the $Co_2(CO)_6$ units are coordinated to the C≡C bonds of **IIb** in an η^2-mode forming distorted pseudo-Co_2C_2 tetrahedra. The two thiophene rings in **9b** display a *trans* arrangement in order to minimize the steric repulsions between the lone pairs on both sulfur atoms. Slight shortenings of the bonds C(14)–C(15) and C(18)–C(19) [1.43(3) and 1.41(3) Å, respectively] are consistent with a partial π component.

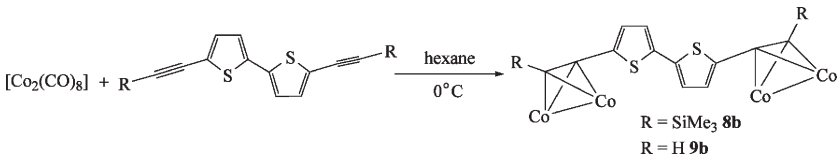

Scheme 5. Synthesis of compounds 8b and 9b.

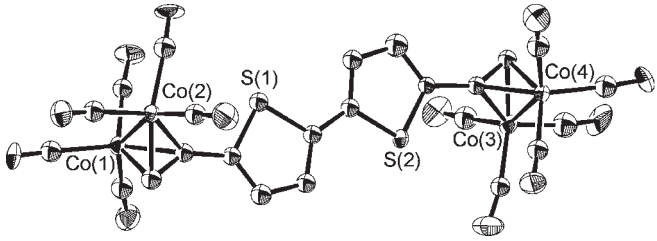

Figure 16. Molecular structure of **9b**.

Both complexes are electroactive as revealed by cyclic voltammetry. The $Co_2(CO)_6$ entity bound to an alkyne was reported by Robinson *et al.* to undergo an irreversible reduction at potentials in the range -0.65 to -1.10 V *vs* Ag/AgCl in CH_2Cl_2 at room temperature.[39] We observed this cobalt cluster based reduction at about -1.58 V *vs* Fc/Fc^+ couple in CH_2Cl_2 at room temperature for **8b**. At ambient temperature, compound **8b** undergoes an irreversible reduction followed by an oxidation event at 0.62 V due to $[Co(CO)_4]^-$ resulting from decomposition of the electrogenerated monoanion.[39,40] At first sight, it looks like no electrochemically detectable electronic communication between the Co_2 cores. In fact, it was shown that the fast chemical decomposition following the redox process in **8b** prevents proper electrochemical analysis.

Low-temperature voltammetric response of **8b** at $-78°C$ displays two well-resolved chemically reversible one-electron couples for the reduction wave with a splitting of 430 mV. Such an observation suggests that, despite the two redox centers being identical, they are coupled from an electronic perspective. These values may be compared with the smaller splitting of 220 mV found in $[\{Co_2(CO)_6\}_2(PhC{\equiv}C{-}C{\equiv}CPh)]$[40] and this indicates that the presence of bithienyl ring within the diyne ligand tends to increase the electronic communication between the two Co_2 moieties.

7. FERROCENYL ACETYLIDES

Research in the development of carbon-rich organometallics containing rigid, π-conjugated chains is burgeoning and of great current interest due to their widespread applications in the syntheses of unsaturated organic species, organometallic polymers, and π-conjugated bi- or multimetallic systems.[41] Molecular wires comprising mixed-valence bimetallic fragments or remote electroactive organometallic building blocks

assembled with all-carbon chains could be used in molecular electronics, optoelectronic devices and chemical sensing appliances.[42] Two models are commonly employed to evaluate the capability of electronic communication between two terminal metal centers "M_1" made possible by an organic spacer "M_1-spacer$-M_1$", and the influence of an organometallic fragment "M_2" in a conjugated organic chain "M_1-spacer$-M_2-$spacer$-M_1$". In several cases, redox-active sites are strongly coupled electronically through the polyynyl fragments.[43] Within this framework, the use of ferrocenyl electrophores and their derivatives offers fascinating perspectives for the design and realization of such molecular wires, due to their stability in both the neutral and oxidized forms. Following our fruitful results on the platinum(II), gold(I), mercury(II) and cobalt(0) acetylide systems, we have expanded our work to some platinum(II) complexes of oligothiophene-functionalized ferrocenylacetylene.[44]

Scheme 6 summarizes the reaction steps leading to the new ferrocenyl compounds in our study. The bromo ferrocenyl derivatives **11a–11c** were prepared in good yields by the Sonogashira coupling reactions of ethynylferrocene with an excess of the corresponding dibromothiophenes.[45] Complexes **10a–10c** were also formed as minor products in these preparations. Analogous cross-coupling reactions of **11a–11c** with trimethylsilylacetylene readily afforded **12a–12c**. Removal of the Me_3Si groups in **12a–12c** to form **13a–13c** was accomplished by treatment with K_2CO_3 in MeOH, which can then be used as key synthons to the hetero-bimetallic and trimetallic systems. The dehydrohalogenation reactions between **13a–13c** and *trans*-[$Pt(PEt_3)_2PhCl$] or *trans*-[$Pt(PBu_3)_2Cl_2$] under the $CuI/^iPr_2NH$ condition provided **14a–14c** and **15a–15c**, respectively, as air-stable red crystalline solids in high yields.

For the crystal structure of **10b**, two halves of the molecules are related by the center of symmetry with an iron–iron through-space distance of *ca.* 17 Å (Figure 17). For **14b**, the bithienyl ligand **IIb** links a ferrocenyl unit at one end and a $Pt(PEt_3)_2Ph$ unit at the other extreme (Figure 18). The two PEt_3 groups adopt a *trans* geometry at the Pt center. All four five-membered rings within the molecule are nearly coplanar (dihedral angles $0.1-11.4^\circ$) and the phenyl ring is inclined by *ca.* 52° to the S(2) thienyl mean plane. For **15b**, the crystal structure shows a diferrocenyl end-capped molecule in which the two acetylide linkages are bonded to the central square-planar Pt center in a *trans* orientation (Figure 19). On steric grounds, the bithienyl systems exhibit a *trans*

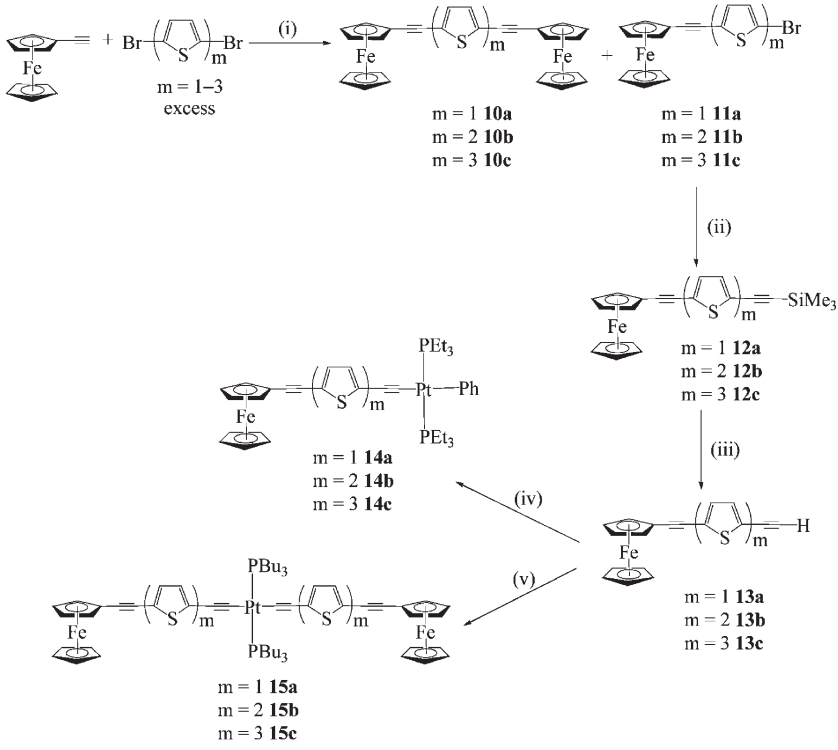

Scheme 6. Synthesis of some platinum (II) complexes of oligothiophene-functionalized ferrocenylacetylene (i) $Pd(OAc)_2$, PPh_3, CuI, $^iPr_2NH$; (ii) $Me_3SiC{\equiv}CH$, $Pd(OAc)_2$, PPh_3, CuI, $^iPr_2NH$; (iii) K_2CO_3, MeOH; (iv) *trans*-$[Pt(PEt_3)_2PhCl]$, $^iPr_2NH$, CuI; (v) *trans*-$[Pt(PBu_3)_2Cl_2]$, $^iPr_2NH$, CuI.

conformation for the sulfur atoms and do not deviate significantly from planarity (mean deviation of *ca*. 0.019–0.035 Å). A slight lengthening of the alkynyl bond lengths (mean distance = 1.22(2) Å) suggests

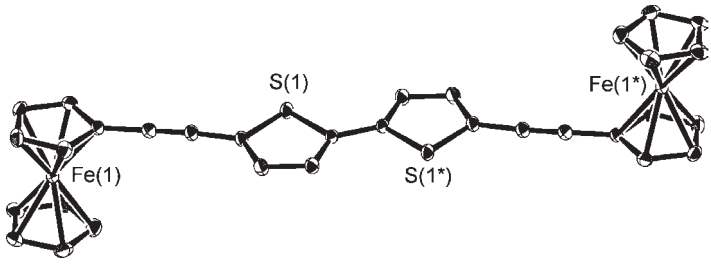

Figure 17. Molecular structure of **10b**.

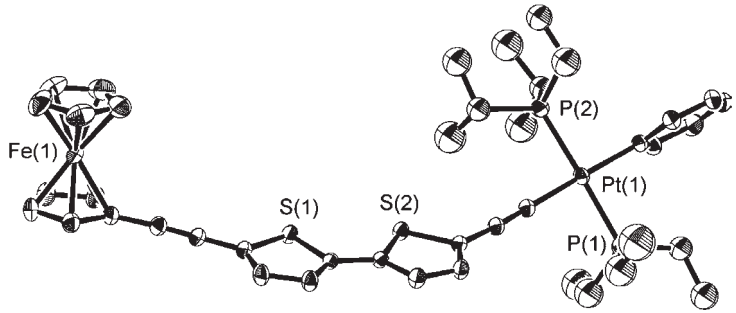

Figure 18. Molecular structure of **14b**.

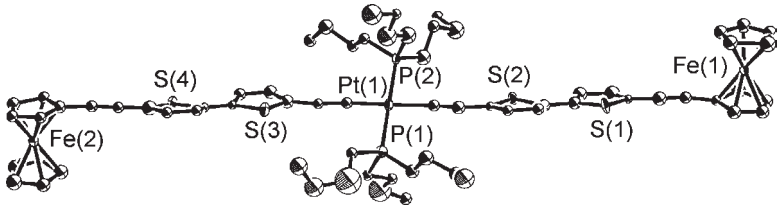

Figure 19. Molecular structure of **15b**.

π-conjugation along the main chain. The rigidity of the complex is confirmed with four C≡C bonds and four thienyl rings connecting the metallated groups to give an iron–iron through-space separation of *ca*. 32 Å.

In general, the absorption spectra of complexes **10–13** show intense, relatively high-energy bands in the near UV and visible region, which arise from $\pi-\pi^*$ transition of the oligothienyl fragments (Table 6). This assignment agrees with the fact that an increase in the extent of π-conjugation with additional thienyl units from one to three results in bathochromic shift of the $\pi-\pi^*$ transition and a notable increase in the molecular extinction coefficients. Increasing the value of m in the main chain stabilizes the LUMO of oligothiophene linkage. The electronic spectra of **14a–14c** and **15a–15c** are also dominated by the structureless $\pi-\pi^*$ transition bands of the organic bridges. The presence of the Pt(II) moiety is found to lower the transition energies and to increase the absorption intensity, indicating an enhancement in the degree of π-delocalization through the Pt conjugated system. Again, increasing conjugation through more thienyl units leads to a decreased transition energy for **14a–14c** as well as **15a–15c**. Thus, a red-shift of *ca*. 61 nm is

Table 6. Electronic absorption and redox data for ferrocenyl compounds

Compound	$\lambda_{max}(\varepsilon/10^3\ M^{-1}\ cm^{-1})^a$	Optical gap/eV[b]	$E_{ox}/V(\Delta E_p)^c$
11a	311 (5.0), 445sh (0.3)	3.12	0.15 (119)
11b	355 (14.4), 460sh (1.2)	3.03	0.12 (119)
11c	394 (43.3)	2.74	0.11 (119), 0.82[d]
12a	327 (17.1), 442sh (1.0)	3.04	0.16 (160)
12b	374 (30.1)	2.90	0.11 (139)
12c	405 (39.3)	2.63	0.10 (80), 0.80[d]
13a	319 (7.1), 429sh (0.6)	2.99	0.16 (139)
13b	369 (29.0)	2.92	0.11 (99)
13c	404 (40.7)	2.64	0.08 (119), 0.72[d]
14a	368 (24.3), 421 (1.4)	2.93	0.12 (99), 0.67[d]
14b	405 (32.9)	2.75	0.10 (119), 0.53[d]
14c	429 (35.9)	2.49	0.06 (119), 0.38[d], 0.70[d]
15a	383 (71.3)	2.90	0.07 (99), 0.65[d]
15b	421 (89.4)	2.57	0.04 (116), 0.51[d]
15c	440 (101.5)	2.44	0.02 (120), 0.35[d], 0.61[d]
10a	340 (26.7), 445sh (3.4)	2.91	[e]
10b	385 (32.4)	2.72	[e]
10c	412 (44.7)	2.46	[e]

[a]In CH_2Cl_2.

[b]Estimated from the absorption edge.

[c]All the potential values are with reference to the external ferrocene standard. $E_{ox} = (E_{pc} + E_{pa})/2$ for reversible oxidation, and peak potential is reported for irreversible oxidation (in volts). ΔE_p in mV. Scan rate = 100 mV s^{-1}.

[d]Irreversible wave.

[e]Ref. 43 h.

observed from **14a** to **14c**, whereas the shift is 57 nm from **15a** to **15c**. We note that λ_{max} decreases according to the sequence **15** > **14** > **10** > **12** > **13** > **11**. However, the extent of bathochromic shifts induced by the end substitution of organometallic groups is less pronounced with an increase in the m value. This substituent effect diminishes progressively as more thienyl units are added and there would be little advantage in increasing the number of thiophene units above 5 or 6. Such chain length dependence of the optical properties can be rationalized from the plot of $\Delta\lambda$ against m (Figure 20) where $\Delta\lambda$ corresponds to the red-shift in wavelength between the organometallic end-substituted complexes **10**, **14** and **15** and the free alkynes **13**. It is obvious that the shift is the largest for **15a–15c** at the same value of m.

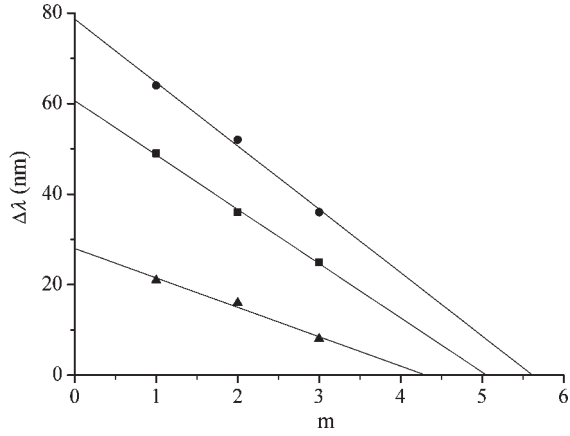

Figure 20. Bathochromic shifts of the absorption maximum induced by the end ferrocenyl substitution (▲), end $-Pt(PEt_3)_2Ph$ substitution (■) and end $-Pt(PBu_3)_2-$ substitution (●), relative to the number of thiophene rings, m, of the chain.

In each case, the cyclic voltammogram is characterized by a single quasi-reversible oxidation wave due to the ferrocenyl electrophore that is present (Table 6). An anodic shift of the Fc/Fc^+ couple with respect to the ferrocene standard is in line with the unsaturation of the ethynyl bridge, which makes the removal of electron more difficult than ferrocene. A small negative shift of the ferrocenyl redox potential occurs upon progressive insertion of thienyl rings because of the increased electron density in the ferrocene vicinity induced by the electron-rich thiophene groups. When the conjugation length is increased, oxidation is favored by the delocalization of charge along the system, which renders the ferrocenyl oxidation easier. Likewise, the slight but notable cathodic shift of the Fe(III)/Fe(II) couple for **14** and **15** can be attributed to the electron delocalization into the Pt segment through a $d\pi \rightarrow p\pi$ interaction. Experimentally, the first oxidation wave for each of **15a–15c** corresponds to a single-step two-electron oxidation involving the concomitant oxidation of the two terminal ferrocenyl moieties. Analogous to **10b**, these two ferrocenyl end groups only exhibit sparse electrocommunication in **15a–15c**. Similar non-interacting diferrocenyl molecules are not unprecedented in the literature and, in fact, are quite common.[40,46]

Another redox event was also observed at higher positive potentials in several compounds due to the oxidation of thienyl fragments. No such anodic wave was associated with compounds **11a**, **11b**, **12a**, **12b**, **13a**

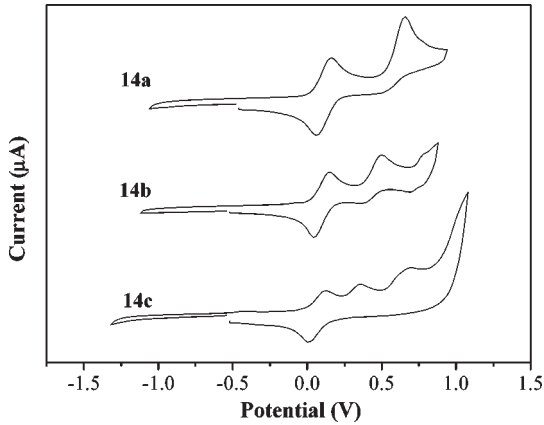

Figure 21. Cyclic voltammograms of **14a–14c** in CH_2Cl_2 (scan rate = 100 mV s^{-1}).

and **13b** with one or two thiophene units. However, complexes **11c**, **12c** and **13c** with an increased oligothienyl chain length were found to undergo an irreversible thienyl oxidation peaking at 0.82, 0.80 and 0.72 V, respectively, which agrees with the common phenomenon that formation of the heteroaromatic cation radicals is favored by the presence of electron-donating end groups[47] and increased conjugation chain.[48] It is well-documented that electrooxidation of oligothiophenes is often an irreversible process because the electrogenerated radical cations readily undergo rapid coupling reactions leading to higher oligomers or polymers. The stability of these radical cations increases when the oligomeric chain becomes longer.[48] Insertion of Pt(II) moieties in **14** and **15** also tends to facilitate the oxidation processes of the thienyl core. For **14a–14c** or **15a–15c**, each of them displays an irreversible thienyl oxidation wave within $0.38-0.67$ V for **14** and $0.35-0.65$ V for **15**, and a second irreversible oxidation of the thiophene moiety also occurs at 0.70 and 0.61 V for **14c** and **15c**, respectively (Figure 21). The waves become more reversible at higher scan rates (>100 mV s^{-1}). Lowering of the redox potential of the thiophene units on increasing the chain length can be verified for **14a–14c** as well as **15a–15c**, which is a manifestation of a more π-delocalized system in the terthienyl congeners. As observed for some thienylenevinylene oligomers, it is likely that the first thienyl oxidation step is generally followed by chemical reactions or the formation of a polymer.[49]

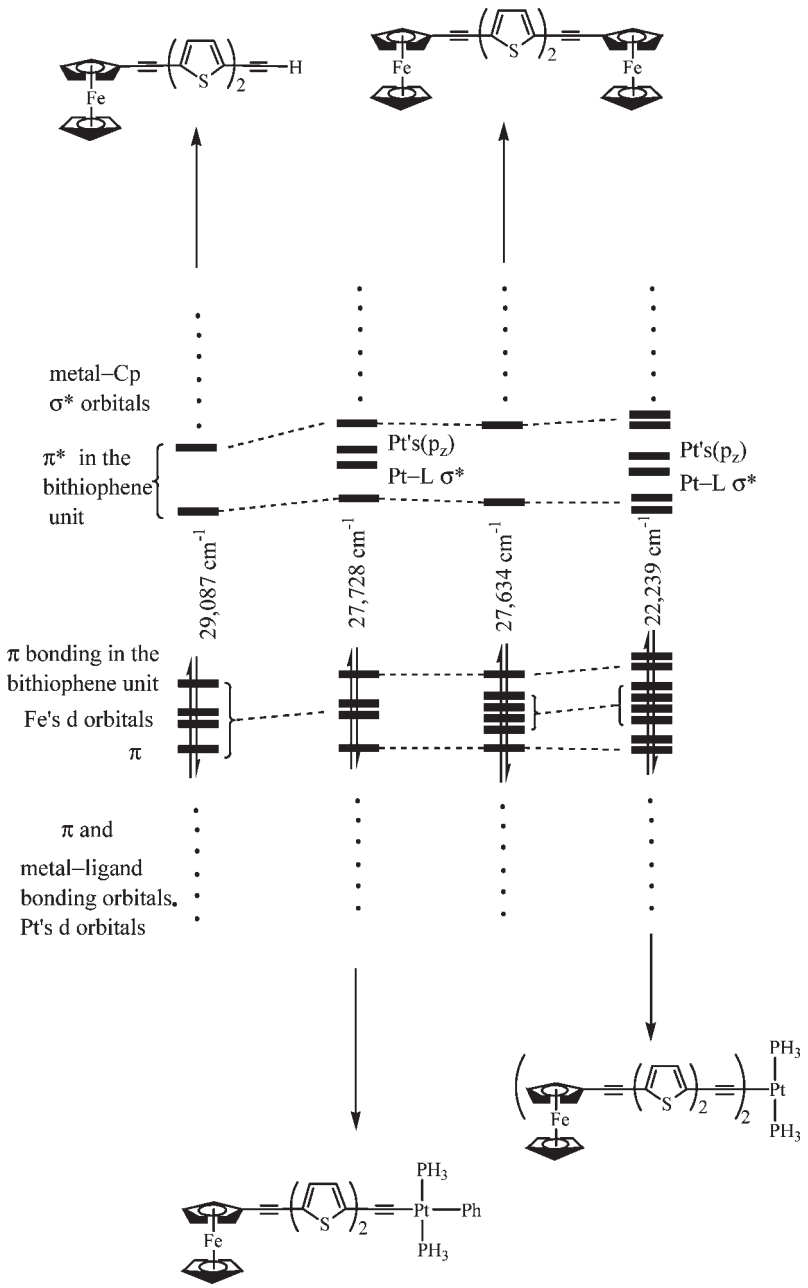

Figure 22. Bonding characteristics of the frontier molecular orbitals for the bithienyl-bridged ferrocenyl complexes.

Molecular orbital calculations at the B3LYP level of density functional theory were carried out for **10b**, **13b**, **14b** and **15b** to study their electronic structures. As illustrated in Figure 22, the HOMO–LUMO transition is related to the $\pi-\pi^*$ excitation within the bithiophene structural unit(s) for each of them. There are two Fe's *d* orbitals immediately below the HOMO which may give rise to high-energy Fe(*d*)-to-ligand(π^*) charge-transfer transition. For **14b** and **15b**, the energy levels are complicated because of the presence of Pt–L(σ^*) components and the Pt's empty *p* orbital in the LUMO region. So, it is likely to observe ligand(π)-to-Pt charge transfer in the UV/VIS spectra at high energies. The increase of π-delocalization by extending the conjugation system or introducing the metal coordination results in a smaller HOMO–LUMO gap. The calculated relative HOMO–LUMO gaps are consistent with the experimental energy gap order **13b** > **14b** > **10b** > **15b** and complex **15b** absorbs at the longest wavelength among the homologous bithiophene family.

8. CONCLUDING REMARKS AND FUTURE DIRECTIONS

We have demonstrated that a series of soluble oligothiophene- and bithiazole-substituted metallaynes can be synthesized in good yields and their spectroscopic and structural properties carefully examined. Electronic absorption, photophysical and redox properties of these compounds have been investigated in terms of the identity of metal groups, the oligothienyl chain length and the electronic nature of the five-membered heterocycle. Addition of metal moieties on the oligothiophene bridges decreases the transition energy of the absorption bands, which is consistent with the theoretical calculations. Crystallographic analyses revealed the formation of polymeric metal acetylide systems in the solid state through d^{10}-d^{10} metal–metal and ligand–ligand interactions for the gold(I) and the isoelectronic mercury(II) centers. Metal-based polythiophene systems can lead the way to new unique electronic and optical materials, and to novel nanomaterials. As well-defined functional materials become more readily available, new structure-property relationships will continue to unfold through systematic studies of structure/physical property correlations. This will allow chemists, physicists, materials scientists, and engineers to have a better grasp on the development of new technologies. Accumulation of the knowledge to understand how to gain control over the structure, properties and function in

polythiophenes would make the synthesis of polythiophenes a critcal subject in the development of new advanced materials. This of course leads to the exciting prospect that the properties of metallated polythiophenes can be selectively engineered through synthesis and assembly.

ACKNOWLEDGEMENTS

I would like to express my sincere thanks to all the postgraduate students and postdoctoral researchers who were involved in this work. I gratefully acknowledge the financial support from the Research Grants Council of the Hong Kong SAR (HKBU2048/01P) and the Hong Kong Baptist University. Thanks are also due to Drs. K.-W. Cheah and Z. Lin and Prof. P. R. Raithby for various kinds of collaborative efforts that were essential for this work.

REFERENCES

1. (a) Nuguyen, P., P. Gómez-Elipe, and I. Manners, 1999. *Chem. Rev.*, **99**, 1515. (b) Kingsborough, R. P. and T. M. Swager, 1999. *Prog. Inorg. Chem.*, **48**, 123.
2. (a) McCullough, R. D. 1998. *Adv. Mater.*, **10**, 93. (b) Skotheim, T. A., R. L. Elsenbaumer, and J. R. Reynolds, 1998. Handbook of Conducting Polymers, Marcel Dekker, New York. (c) Stott, T. L. and M. O. Wolf, 2003. *Coord. Chem. Rev.*, **246**, 89. (d) Hirao, T. 2002. *Coord. Chem. Rev.*, **226**, 81.
3. (a) Bredas, J. L. and R. R. Chance, (Eds.), 1990. Conjugated Polymer Materials: Opportunities in Electronic, Optoelectronic and Molecular Electronics, Kluwer Academic Publishers, Dordrecht. (b) Garnier, F. 1999. *Acc. Chem. Res.*, **32**, 209.
4. (a) Kraft, A., A. C. Grimsdale, and A. B. Holmes, 1998. *Angew. Chem. Int. Ed.*, **37**, 402. (b) Gigli, G., G. Barbarella, L. Favaretto, F. Cacialli, and R. Cingolani, 1999. *Appl. Phys. Lett.*, **75**, 439. (c) Barbarella, G., L. Favaretto, G. Sotgiu, M. Zambianchi, V. Fattori, M. Cocchi, F. Cacialli, G. Gigli, and R. Cingolani, 1999. *Adv. Mater.*, **11**, 1375. (d) Gigli, G., O. Inganas, M. Anni, M. DeVittorio, R. Cingolani, G. Barbarella, and L. Favaretto, 2001. *Appl. Phys. Lett.*, **78**, 1493.
5. (a) Barbarella, G. 2002. *Chem. Eur. J.*, **8**, 5073. (b) MacEachern, A., C. Soucy, L. C. Leitch, J. T. Arnason, and P. Morand, 1988. *Tetrahedron*, **44**, 2403.
6. (a) Guay, J., P. Kasai, A. Diaz, R. Wu, L. H. Dao, and J. M. Tour, 1992. *Chem. Mater.*, **4**, 1097. (b) Garnier, F., A. Yassar, R. Hajlaoui, G. Horowitz, F. Deloffre, B. Servet, S. Ries, and P. Alnot, 1993. *J. Am. Chem. Soc.*, **115**, 8716. (c) Bauerle, P. 1992. *Adv. Mater.*, **4**, 102.

7. (a) Bunz, U. H. F. 2000. *Chem. Rev.*, **100**, 1605. (b) Long, N. J. and C. K. Williams, 2003. *Angew. Chem. Int. Ed.*, **42**, 2586.
8. (a) Yu, W.-L., H. Meng, J. Pei, Y.-H. Lai, S.-J. Chua, and W. Huang, 1998. *Chem. Commun.*, 1957. (b) Nakanishi, H., N. Sumi, A. Yoshio, and T. Otsubo, 1998. *J. Org. Chem.*, **63**, 8632. (c) Jestin, I., P. Frère, N. Mercier, E. Levillain, D. Stievenard, and J. Roncali, 1998. *J. Am. Chem. Soc.*, **120**, 8150. (d) Graf, D. D. and K. R. Mann, 1997. *Inorg. Chem.*, **36**, 150. (e) Graf, D. D., R. G. Duan, J. P. Campbell, L. L. Miller, and K. R. Mann, 1997. *J. Am. Chem. Soc.*, **119**, 5888. (f) Mitschke, U., E. Mena Osteritz, T. Debaerdemaeker, M. Sokolowski, and P. Bäuerle, 1998. *Chem. Eur. J.*, **4**, 2211.
9. (a) Pollagi, T. P., T. C. Stoner, R. F. Dallinger, T. M. Gilbert, and M. D. Hopkins, 1991. *J. Am. Chem. Soc.*, **113**, 703. (b) Calabrese, J. C., L.-T. Cheng, J. C. Green, S. R. Marder, and W. Tam, 1991. *J. Am. Chem. Soc.*, **113**, 7227. (c) Meyers, L. K., C. Langhoff, and M. E. Thompson, 1992. *J. Am. Chem. Soc.*, **114**, 7560. (d) Lichtenberger, D. L., S. K. Renshaw, and R. M. Bullock, 1993. *J. Am. Chem. Soc.*, **115**, 3276. (e) Manners, I. 1996. *Angew. Chem., Int. Ed. Engl.*, **35**, 1602.
10. (a) Nanos, J. I., J. W. Kampf, and M. D. Curtis, 1995. *Chem. Mater.*, **7**, 2232. (b) Yamamoto, T., H. Suganuma, T. Maruyama, T. Inoue, Y. Muramatsu, M. Arai, D. Komarudin, N. Ooba, S. Tomaru, S. Sasaki, and K. Kubota, 1997. *Chem. Mater.*, **9**, 1217.
11. Lewis, J., N. J. Long, P. R. Raithby, G. P. Shields, W.-Y. Wong, and M. Younus, 1997. *J. Chem. Soc., Dalton Trans.*, 4283.
12. Wong, W.-Y., S.-M. Chan, K.-H. Choi, K.-W. Cheah, and W.-K. Chan, 2000. *Macromol. Rapid Commun.*, **21**, 453.
13. Wong, W.-Y., K.-H. Choi, G.-L. Lu, and Z. Lin, 2002. *Organometallics*, **21**, 4475.
14. Ahrens, B., K.-H. Choi, M. S. Khan, P. Li, P. R. Raithby, P. J. Wilson, and W.-Y. Wong, 2002. *Cryst. Eng. Comm.*, **4**, 405.
15. (a) Sonogashira, K., Y. Fujikura, T. Yatake, N. Toyoshima, S. Takahashi, and N. Hagihara, 1978. *J. Organomet. Chem.*, **145**, 101. (b) Sonogashira, K., S. Kataoka, S. Takahashi, and N. Hagihara, 1978. *J. Organomet. Chem.*, **160**, 319.
16. Chawdhury, N., A. Köhler, R. H. Friend, W.-Y. Wong, J. Lewis, M. Younus, P. R. Raithby, T. C. Corcoran, M. R. A. Al-Mandhary, and M. S. Khan, 1999. *J. Chem. Phys.*, **110**, 4963. (b) Chawdhury, N., A. Köhler, R. H. Friend, M. Younus, N. J. Long, P. R. Raithby, and J. Lewis, 1998. *Macromolecules*, **31**, 722.
17. Sease, J. W. and L. Zechmeister, 1947. *J. Am. Chem. Soc.*, **69**, 270.
18. Wittmann, F., R. H. Friend, M. S. Khan, and J. Lewis, 1994. *J. Chem. Phys.*, **101**, 2693.
19. Wittmann, H. F., K. Fuhrmann, R. H. Friend, M. S. Khan, and J. Lewis, 1993. *Synth. Met.*, **55–57**, 56.

20. Cornil, J., D. Beljonne, D. A. dos Santos, Z. Shuai, and J. L. Bredas, 1996. *Synth. Met*., **78**, 209.
21. Beljonne, D., J. Cornil, J. L. Bredas, and R. H. Friend, 1996. *Synth. Met*., **76**, 61.
22. Köhler, A., D. A. dos Santos, D. Beljonne, Z. Shuai, J. L. Bredas, R. H. Friend, A. B. Holmes, A. Kraus, and K. Müllen, 1998. *Nature (London*)., **392**, 903.
23. Younus, M., A. Köhler, S. Cron, N. Chawdhury, M. R. A. Al-Mandhary, M. S. Khan, J. Lewis, N. J. Long, R. H. Friend, and P. R. Raithby, 1998. *Angew. Chem. Int. Ed*., **37**, 3036.
24. (a) Köhler, A., F. Wittmann, R. H. Friend, M. S. Khan, and J. Lewis, 1994. *Synth. Met*., **67**, 245. (b) Tang, C. W. and A. C. Albrecht, 1974. *J. Chem. Phys*., **62**, 2139. (c) Marks, R. N., J. J. M. Halls, D. D. C. Bradley, R. H. Friend, and A. B. Holmes, 1994. *J. Phys. Condens. Matter*, **6**, 1379.
25. Harrison, M. G., J. Gruner, G. C. W. Spencer, 1997. *Phys. Rev. B*., **55**, 7831.
26. Graham, S. C. 1995. Ph.D. Thesis, University of Cambridge.
27. (a) Shieh, S. J., X. Hong, S. M. Peng, and C. M. Che, 1994. *J. Chem. Soc., Dalton Trans*., 3067. (b) Tzeng, B. C., W. C. Lo, C. M. Che, and S. M. Peng, 1996. *Chem. Commun*., 181. (c) Puddephatt, R. J. 1998. *Chem. Commun*., 1055. (d) Yam, V.-W. W. and K. K.-W. Lo, 1999. *Chem. Soc. Rev*., **28**, 323.
28. (a) Whittall, I. R., M. G. Humphrey, S. Houbrechts, and A. Persoons, 1996. *Organometallics*., **15**, 5738. (b) Whitall, I. R., M. G. Humphrey, M. Samoc, and B. Luther-Davies, 1997. *Angew. Chem., Int. Ed. Engl*., **36**, 370. (c) Houbrechts, S., C. Boutton, K. Clays, A. Persoons, I. R. Whittall, R. H. Naulty, M. P. Cifuentes, and M. G. Humphrey, 1998. *J. Nonlinear Opt. Phys. and Mater*., **7**, 113. (d) McDonagh, A. M., N. T. Lucas, M. P. Cifuentes, M. G. Humphrey, S. Houbrechts, and A. Persoons, 2000. *J. Organomet. Chem*., **605**, 193.
29. Li, D., X. Hong, C. M. Che, W. C. Lo, and S. M. Peng, 1993. *J. Chem. Soc., Dalton Trans*., 2929.
30. Irwin, M. J., J. J. Vittal, and R. J. Puddephatt, 1997. *Organometallics*, **16**, 3541.
31. Birks, J. B. 1970. *Photophysics of Aromatic Molecules*, Wiley-Interscience, London.
32. Hoffmann, R. 1982. *Angew. Chem., Int. Ed. Engl*., **21**, 711.
33. Wong, W.-Y., K.-H. Choi, G.-L. Lu, J.-X. Shi, P.-Y. Lai, S.-M. Chan, and Z. Lin, 2001. *Organometallics*, **20**, 5446.
34. (a) Gutierrez-Puebla, E., A. Vegas, and S. Garcia-Blanco, 1978. *Acta Crystallogr. Sect. B*., **34**, 3382. (b) Hoskins, B. F., R. Robson, and E. E. Sutherland, 1996. *J. Organomet. Chem*., **515**, 259. (c) Hartbaum, C., G. Roth, and H. Fischer, 1998. *Eur. J. Inorg. Chem*., 191. (d) Ghosh, I., R. Mishra, D. Poddar, and A. K. Mukherjee, 1996. *Chem. Commun*., 435. (e) Faville, S. J.,

W. Henderson, T. J. Mathieson, and B. K. Nicholson, 1999. *J. Organomet. Chem*., **580**, 363. (f) Wong, W.-Y., G.-L. Lu, L. Liu, J.-X. Shi, and Z. Lin, 2004. *Eur. J. Inorg. Chem*., 2066.

35. Diez, R. P., *MullPop Program*, National University of La Plata, Argentina.
36. Bolletta, F., D. Fabbri, M. Lombardo, L. Prodi, C. Trombini, and N. Zaccheroni, 1996. *Organometallics*., **15**, 2415.
37. (a) Housecroft, C. E., B. F. G. Johnson, M. S. Khan, J. Lewis, P. R. Raithby, M. E. Robson, and D. A. Wilkinson, 1992. *J. Chem. Soc., Dalton Trans*., 3171. (b) Draper, S. M., M. Delamesiere, E. Champeil, B. Twamley, J. J. Byrne, and C. Long, 1999. *J. Organomet. Chem*., **589**, 157. (c) Verdaguer, X., A. Moyano, M. A. Pericàs, A. Riera, A. Alvarez-Larena, and J.-F. Piniella, 1999. *Organometallics*., **18**, 4275.
38. Wong, W.-Y., H.-Y. Lam, and S.-M. Lee, 2000. *J. Organomet. Chem*., **595**, 70.
39. (a) Worth, G. H., B. H. Robinson, and J. Simpson, 1992. *Organometallics*., **11**, 3863. (b) Worth, G. H., B. H. Robinson, and J. Simpson, 1990. *J. Organomet. Chem*., **387**, 337.
40. Osella, D., L. Milone, C. Nervi, and M. Ravera, 1995. *J. Organomet. Chem*., **488**, 1.
41. (a) De Meijere, A. (Ed.) 1999. Carbon-Rich Compounds II: Macrocyclic Oligoacetylenes and Other Linearly Conjugated Systems, Springer, Berlin, Germany. (b) Adams, R. D. and U. H. F. Bunz, 2003. Carbon-Rich Organometallic Compounds in the Special Issue of the Journal of Organometallic Chemistry, Elsevier, Amsterdam, The Netherlands.
42. (a) Ziessel, R., M. Hissler, A. El-Ghayoury, and A. Harriman, 1998. *Coord. Chem. Rev.*, **178–180**, 1251. (b) Balzani, V., A. Juris, M. Venturi, S. Campagna, and S. Serroni, 1996. *Chem. Rev*., **96**, 759. (c) Paul, F. and C. Lapinte, 1998. *Coord. Chem. Rev.*, **178–180**, 431. (d) Ward, M. D. 1995. *Chem. Soc. Rev.*, 121. (e) Barlow, S. and D. O'Hare, 1997. *Chem. Rev.*, **97**, 637.
43. (a) Schimanke, H. and R. Gleiter, 1998. *Organometallics*., **17**, 275. (b) Justin Thomas, K. R., J. T. Lin, and K.-J. Lin, 1999. *Organometallics*., **18**, 5285. (c) Hradsky, A., B. Bildstein, N. Schuler, H. Schottenberger, P. Jaitner, K.-H. Ongania, K. Wurst, and J.-P. Launay, 1997. *Organometallics*., **16**, 392. (d) Stang, S. L., F. Paul, and C. Lapinte, 2000. *Organometallics*., **19**, 1035. (e) Brady, M., W. Weng, and J. A. Gladysz, 1994. *J. Chem. Soc., Chem. Commun*., 2655. (f) Justin Thomas, K. R., J. T. Lin, and Y. S. Wen, 1999. *J. Organomet. Chem*., **575**, 301. (g) Jones, N. D., M. O. Wolf, and D. M. Giaquinta, 1997. *Organometallics*., **16**, 1352. (h) Justin Thomas, K. R., J. T. Lin, and Y. S. Wen, 2000. *Organometallics*., **19**, 1008. (i) Colbert, M. C. B., J. Lewis, N. J. Long, P. R. Raithby, A. J. P. White, and D. J. Williams, 1997. *J. Chem. Soc., Dalton Trans*., 99. (j) Adams, R. D., B. Qu, and M. D. Smith, 2002. *Organometallics*., **21**, 4847.

44. Wong, W.-Y., G.-L. Lu, K.-F. Ng, K.-H. Choi, and Z. Lin, 2001. *J. Chem. Soc., Dalton Trans*., 3250.
45. (a) Sonogashira, K., Y. Tohda, and N. Hagihara, 1975. *Tetrahedron Lett*., 4467. (b) Takahashi, S., Y. Kuroyama, K. Sonogashira, and N. Hagihara, 1980. *Synthesis*, 627.
46. (a) Osella, D., R. Gobetto, C. Nervi, M. Ravera, R. D'Amato, and M. V. Russo, 1998. *Inorg. Chem. Commun*., **1**, 239. (b) Lavastre, O., J. Plass, P. Bachmann, A. Salaheddine, C. Moinet, and P. H. Dixneuf, 1997. *Organometallics*, **16**, 184.
47. Bäuerle, P. 1992. *Adv. Mater.*, **4**, 102.
48. Garcia, P., J. M. Pernaut, P. Hapiot, V. Wintgens, P. Valat, F. Garnier, and D. Delabouglise, 1993. *J. Phys. Chem*., **97**, 513.
49. Jestin, I., P. Frère, N. Mercier, E. Levillain, D. Stievenard, and J. Roncali, 1998. *J. Am. Chem. Soc*., **120**, 8150.